Tailoring the Electrocatalytic Activity and Selectivity of Pt(111) through Cathodic Corrosion

Hersbach, T.J.P.; Ye, C.; Garcia, A.C.; Koper, M.T.M.

DOI
10.1021/acscatal.0c04016

Publication date
2020

Document Version
Final published version

Published in
ACS Catalysis

ACS Catalysis

pubs.acs.org/acscatalysis

Research Article

Tailoring the Electrocatalytic Activity and Selectivity of Pt(111) through Cathodic Corrosion

Thomas J. P. Hersbach,* Chunmiao Ye, Amanda C. Garcia, and Marc T. M. Koper*

Cite This: *ACS Catal.* 2020, 10, 15104–15113

Read Online

ACCESS | Metrics & More | Article Recommendations | Supporting Information

ABSTRACT: Developing active and selective electrocatalysts is of prime importance in shifting society toward utilizing renewable energy sources. Such developments often require catalysts with particular morphologies because many chemical reactions are sensitive to the catalyst structure. However, it can be challenging to synthesize and stabilize shape-controlled catalysts. It would therefore be desirable to tailor the morphology of an existing electrocatalyst to exhibit favorable catalytic properties. In this work, such morphological alteration is explored using cathodic corrosion: an electrochemical etching process that can generate geometrical shapes on metallic surfaces. Specifically, cathodic corrosion is utilized to tailor a well-defined Pt(111) electrode for oxygen reduction and glycerol oxidation catalysis. Both the oxygen reduction activity and the glycerol oxidation selectivity can be tailored by controlling the cathodic corrosion conditions. These results demonstrate the specific potential of cathodic corrosion for tailoring catalyst activity and selectivity.

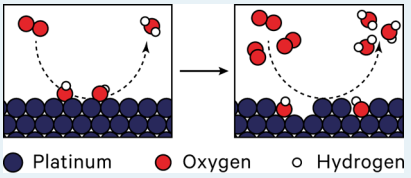

KEYWORDS: *cathodic corrosion, oxygen reduction, glycerol oxidation, catalyst structure, rational catalyst design*

INTRODUCTION

Anthropogenic climate change has stimulated large-scale efforts to shift from fossil to renewable sources of energy.[1,2] A prominent approach for achieving this shift is the electrification of society, in which renewable electricity is stored in batteries[3] or used to electrochemically produce "green" fuels[4−6] or industrially relevant chemicals.[7−9] Unfortunately, many electrochemical conversions are still limited by the performance of the involved electrocatalyst.[10] It is therefore crucially important to develop more active and selective electrocatalysts.

Electrocatalyst development can be divided into two main strategies: compositional tuning and structural tuning. In compositional tuning, the elemental makeup of a catalyst is varied, often by creating alloy catalysts.[11−13] This strategy is usually guided by theoretical predictions[10,14] and has yielded significant performance improvements in model catalyst systems.[15−18] However, translating model catalysts to their industrially relevant nanoparticle equivalents can be complicated, with many alloy nanoparticles being unstable and changing their composition during catalysis.[5,19−22] It might therefore be more prudent to generate catalysts from single elements.

Single-element catalysts can be enhanced through structural tuning, in which a catalyst's surface structure is tailored to expose sites with favorable catalytic properties.[23,24] This is usually achieved by synthesizing shape-controlled nanoparticles, which often possess well-defined facets.[21] However, rationally synthesizing these particles is not trivial and commonly involves the use of capping agents that adversely affect catalytic performance.[21,25] A more straightforward approach for structural tuning could be to synthesize or purchase non-shape-controlled nanoparticles and subsequently optimize their structure.[26]

Such optimization could be achieved through cathodic corrosion:[27] an electrochemical etching process that can rapidly and drastically alter the structure of metallic surfaces during polarization at cathodic potentials.[28,29] This alteration was recently shown to be tunable, because different surface features can be created by varying the electrolyte in which cathodic corrosion occurs.[30] Such tunability would imply that cathodic corrosion can be applied to preferentially expose active sites on electrocatalysts.

This application of cathodic corrosion is explored in the current work by altering the catalytic activity and selectivity of a Pt(111) electrode. The electrode will be tailored for the oxygen reduction reaction (ORR) and glycerol oxidation. Each of these reactions demonstrates a different type of enhancement: the ORR *activity* of Pt(111) can be enhanced by introducing (localized) defects,[31−33] whereas the glycerol oxidation *selectivity* of Pt is sensitive to the presence of (long-range) (111) and (100) terraces.[34] As will be demonstrated, both types of catalytic performance modification can indeed be realized on a Pt(111) electrode. Such enhancements for a well-defined Pt(111) model system

Received: September 13, 2020
Revised: November 17, 2020
Published: December 7, 2020

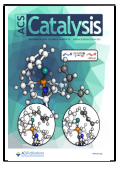

https://dx.doi.org/10.1021/acscatal.0c04016
ACS Catal. 2020, 10, 15104−15113

encourage the use of cathodic corrosion to structurally tune nanoparticle catalysts.

MATERIALS AND METHODS

Cleaning and Sample Preparation. All water used in this work (resistivity > 18.2 MΩ·cm, TOC < 5 ppb) was purified with a Millipore MilliQ system. All glassware was cleaned from organic contamination by soaking overnight in an aqueous solution of 1 $g \cdot L^{-1}$ $KMnO_4$ (Fluka, ACS reagent) and 0.5 M H_2SO_4 (Fluka, ACS reagent). Before experiments, this solution was drained and residual MnO_4^- was decomposed by immersing the glassware in dilute H_2O_2 (Merck, Emprove exp). This solution was subsequently drained and all the glassware was boiled in water six times to remove inorganic contaminations, including (bi)sulfate from the cleaning solution.

After cleaning, two three-electrode glass cells were prepared: one cell for sample characterization and one cell for catalysis. The contents of each cell depended on the purpose of the cell; cells for blank voltammograms and oxygen reduction catalysis were filled with 0.1 M $HClO_4$ (Fluka, TraceSelect), whereas cells for glycerol oxidation catalysis were filled with 0.5 M $HClO_4$ (Fluka, TraceSelect). Each cell contained a Pt counter electrode (Mateck, 99.9%) and an internal reversible hydrogen electrode (RHE) which used a constant hydrogen (Linde, 6.0 purity) flow. The RHE was connected to an auxiliary Pt electrode in the main cell compartment with a 4.7 μF capacitor, in order to reduce high-frequency noise during electrochemical experiments.[35]

In addition to these two glass cells, a third single-compartment cell made of fluorinated ethylene propylene (FEP) was used for cathodic corrosion. This cell was filled with 1 or 10 M NaOH (Merck, Suprapur) or 5 M $LiOH \cdot H_2O$ (Alfa Aesar, 99.995%). The corrosion cell contained a commercial "Hydroflex" RHE (Gaskatel) and a dimensionally stable anode counter electrode provided by Magneto Special Anodes. This rod-shaped anode consisted of titanium, coated with a porous iridium mixed metal oxide. Before use, this electrode was cleaned by rinsing it with H_2O_2 because it could not be cleaned by flame-annealing or soaking in the $KMnO_4$ cleaning solution; annealing would destroy the electrode, whereas soaking led to $KMnO_4$ being absorbed into the porous oxide. This $KMnO_4$ could not be removed by boiling the electrode and would therefore be expelled into the working solution when experiments induced oxygen evolution on the counter electrode. Fortunately, the H_2O_2 rinsing procedure proved adequate in cleaning the electrode because no contamination-induced cathodic corrosion onset potential shifts like those occurring in previous work were observed.[30]

Prior to each experiment, working electrodes were prepared by flame-annealing them with a propane torch for approximately 20 s. Notably, this brief annealing period allowed for complete rejuvenation of the electrode surface, such that a single electrode could be reused for all cathodic corrosion experiments. After annealing, the electrodes were cooled down in a glass cooler in a reducing H_2/Ar (Linde, 6.0 purity) atmosphere. After cooling, the electrodes were protected with a droplet of deoxygenated water from the cooling flask and transferred to one of the electrochemical cells. The electrodes used in this study were a home-made 2.3 mm-diameter bead-type polycrystalline Pt electrode, denoted as Pt(poly); a 2.1 mm-diameter bead-type Pt(100) electrode (iCryst); a 2.5 mm-diameter bead-type Pt(110) electrode (iCryst); and a 3 mm-diameter, 2 mm-high cylindrical Pt(111) crystal (Surface Preparation Laboratory). Cyclic voltammetry (CV) curves for these electrodes are presented in Figure S1.

Electrochemistry. Electrochemical experiments were performed with a Bio-Logic VSP-300 potentiostat. After setting up the glassware, CV was run in both glass cells to ensure the cleanliness of the working solutions. Specifically, each cell was deaerated by purging the electrolyte with argon (Linde, 6.0 purity) for at least 30 min. Then, four CV curves of the Pt(111) electrode were recorded in the hanging meniscus configuration at a scan rate of 50 $mV \cdot s^{-1}$, between 0.06 and 0.9 V versus RHE, while maintaining deaeration by flowing argon over the working electrolyte. In cells used for oxygen reduction, special attention was paid to the presence of (bi)sulfate, which significantly affects the oxygen reduction activity.[36,37] (Bi)sulfate can easily be detected in Pt(111) voltammograms because it causes a distinct reductive feature between 0.45 and 0.55 V versus RHE at concentrations as low as 10^{-6} M.[38] If no signs of (bi)sulfate were present and the voltammograms did not change shape between cycles, the cells were considered to be clean enough for catalysis. After establishing cleanliness, catalytic reagents were added into the cell. For oxygen reduction, the argon flow in the catalysis cell was replaced by O_2 (Linde, 6.0 purity), which was bubbled through the working electrolyte for at least 10 min to ensure oxygen saturation. For glycerol oxidation, glycerol (Merck, Emsure) was added to achieve a concentration of 0.1 M.

Each experiment started by running four Pt(111) CVs in the characterization cell as described above, to validate the cleanliness and ordering of the surface. The Pt(111) electrode was then rinsed and immersed for at least 1 mm in the corrosion cell. In this cell, the cell resistance was determined through impedance spectroscopy at 0.5 V versus RHE, at a 100 kHz frequency and a 20 mV sine wave amplitude.[39] This resistance value was used to subsequently apply an 85% IR-corrected potential to the electrode for 60 s, in order to modify the electrode through cathodic corrosion. Following modification, the electrode was removed under potential control, rinsed, and moved to the characterization cell. In this cell, the state of the electrode surface was characterized by running four CVs between 0.06 and 0.7 V versus RHE. The 0.7 V potential bound was chosen as a safe upper limit where none of the cathodically produced sites would be removed through oxidation of the surface. After characterization, the ORR or glycerol oxidation activity was studied.

The ORR activity was assessed in the hanging meniscus rotating disk (HMRD) configuration.[40] To this end, the electrode was mounted in a home-made electrode holder that was subsequently screwed into the shaft of a Pine rotator. The electrode was lowered into the catalysis cell, where oxygen now flowed over the electrolyte solution to maintain oxygen saturation during experiments. In this cell, a meniscus was made between the electrode and the electrolyte while polarizing the electrode at 0.1 V versus RHE. After making contact, the cell resistance was determined through impedance spectroscopy at 0.9 V versus RHE. This cell resistance was used to apply an 85% IR correction to subsequently applied potentials. The electrode potential was then held at 0.06 V versus RHE for 5 s before testing the catalytic activity of the electrode with cyclic voltammetry; two CVs were run between 0.06 and 0.9 V versus RHE, at a scan rate of 50 $mV \cdot s^{-1}$. The electrode rotation rate was then automatically changed by the potentiostat to 200 rpm, the current was allowed to stabilize

https://dx.doi.org/10.1021/acscatal.0c04016
ACS Catal. 2020, 10, 15104−15113

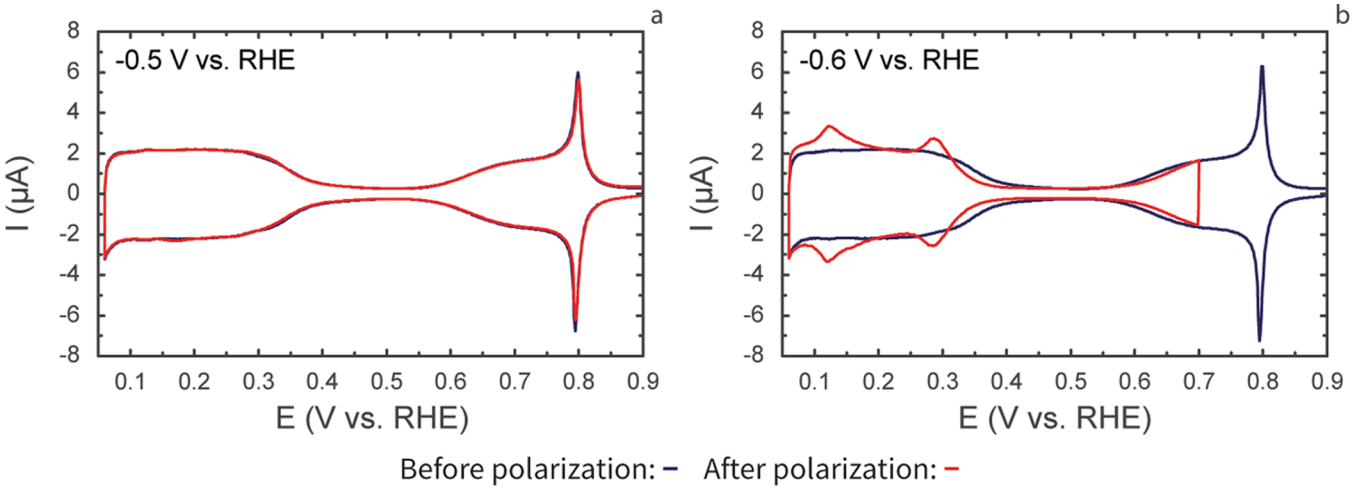

Figure 1. Cyclic voltammograms of Pt(111) before (blue trace) and after (red trace) cathodic polarization in 1 M NaOH at −0.5 V vs RHE (a) and −0.6 V vs RHE (b). Voltammograms were recorded in 0.1 M $HClO_4$ at a scan rate of 50 mV·s^{-1}.

for 5 s at 0.06 V versus RHE, and two CV curves were recorded between 0.06 and 0.9 V versus RHE. This step was repeated to obtain additional CVs at rotation rates of 400, 900, 1600, and 2500 rpm.

The glycerol oxidation activity was studied in the hanging meniscus configuration. A meniscus was made at 0.1 V versus RHE, after which the electrode was equilibrated at 0.06 V versus RHE for 10 s. Following equilibration, the catalytic activity was assessed by running two CV cycles between 0.06 and 0.9 V versus RHE at a scan rate of 10 mV·s^{-1} and one CV cycle between the same potential bounds at 1 mV·s^{-1}. IR correction was found to be unnecessary for glycerol oxidation experiments.

Online High-Performance Liquid Chromatography. Online high-performance liquid chromatography (HPLC) was used to detect the liquid products produced during the electrochemical oxidation of glycerol on Pt(111) before and after cathodic corrosion. All preparatory cleaning and electrode preparation steps for online HPLC were carried out as described above. Some deviations from the previous protocols will be outlined here.

A bigger Pt(111) electrode (Mateck, diameter: 10 mm) was used than that for other catalysis experiments, in order to generate higher concentrations of reaction products. The electrode was corroded without IR correction at −3 V versus RHE. However, an IR drop of 1 V was estimated from the cell resistance, such that the "real" corrosion potential was −2 V versus RHE. Blank voltammograms for this electrode in the uncorroded and corroded state are displayed in Figure S2. The electrode was catalytically tested in an H-cell. Both H-cell compartments were separated with a Nafion 117 membrane (Aldrich, thickness: 0.007 in.). The membrane was pretreated by consecutively boiling in 3% H_2O_2 (Merck, Emprove exp), water, 1 M H_2SO_4 (Fluka, ACS Reagent), and water, for 1 h each.[41] In this cell, catalysis voltammograms for HPLC were recorded using an Autolab PGSTAT12 potentiostat. The followed HPLC procedure resembles previous work[34] but will be outlined below for clarity.

For online HPLC characterization, reaction products were collected during linear voltammetry with a small Teflon tip (inner diameter: 0.38 mm). The tip was positioned approximately 10 μm from the center of the working electrode and was connected to a PEEK capillary (inner diameter: 0.13 mm; outer diameter: 1.59 mm). The tip and capillary were cleaned before sample collection with ultrapure water and the supporting electrolyte. For sample collection, 60 μL of sample was collected on a 96-well microtiter plate (270 μL/well, Screening Devices) using an automatic fraction collector (FRC-10A, Shimadzu). A sample collection flow rate of 60 μL/min was maintained with a Shimadzu pump (LC-20AT). Samples were taken every 60 mV, in the potential range between 0.06 and 0.9 V versus RHE at 1.0 mV s^{-1}. Following sample collection, the microtiter plate was covered by a silicone mat to prevent sample evaporation. The microtiter plate with the collected samples was placed in an auto sampler (SIL-20A) holder, and the samples were analyzed by HPLC (Prominence HPLC, Shimadzu) that utilized its own LC-20AT pump (Shimadzu). A total of 30 μL of each sample was injected into the HPLC system for analysis. The HPLC column configuration featured an Aminex HPX 87-H (BioRad) column together with a Micro-Guard Cation H cartridge (BioRad), in series with a Sugar SH1011 (Shodex) column. Diluted sulfuric acid (5 mM) was used as the eluent. The column temperature was held at 80 °C in a column oven (CTO-20A), and the separated compounds were detected with a refractive index detector (RID-10A). Blank samples of each expected product were analyzed as well, in order to produce standard calibration curves at 80 °C. The analyzed compounds were glyceraldehyde, dihydroxyacetone, glyceric acid, glycolic acid, formic acid, oxalic acid, mesoxalic acid, hydroxypyruvic acid, and tartronic acid.

RESULTS

In this section, we assess the effect of cathodic corrosion and the subsequent change in ORR activity and glycerol oxidation for Pt(111). Each reaction will be considered separately, starting with the ORR.

Oxygen Reduction. The ORR is one of the main performance bottlenecks in fuel cells,[42] with even active catalysts such as platinum being limited in their performance.[43] Platinum and related catalysts bind reaction intermediates such as adsorbed hydroxide (*OH) too strongly:[42] calculations indicate *OH binding on Pt(111) to be approximately 0.1 eV too strong.[19] This would suggest that weakening the Pt−OH bond can enhance the electrocatalytic activity of Pt.[13]

https://dx.doi.org/10.1021/acscatal.0c04016
ACS Catal. 2020, 10, 15104−15113

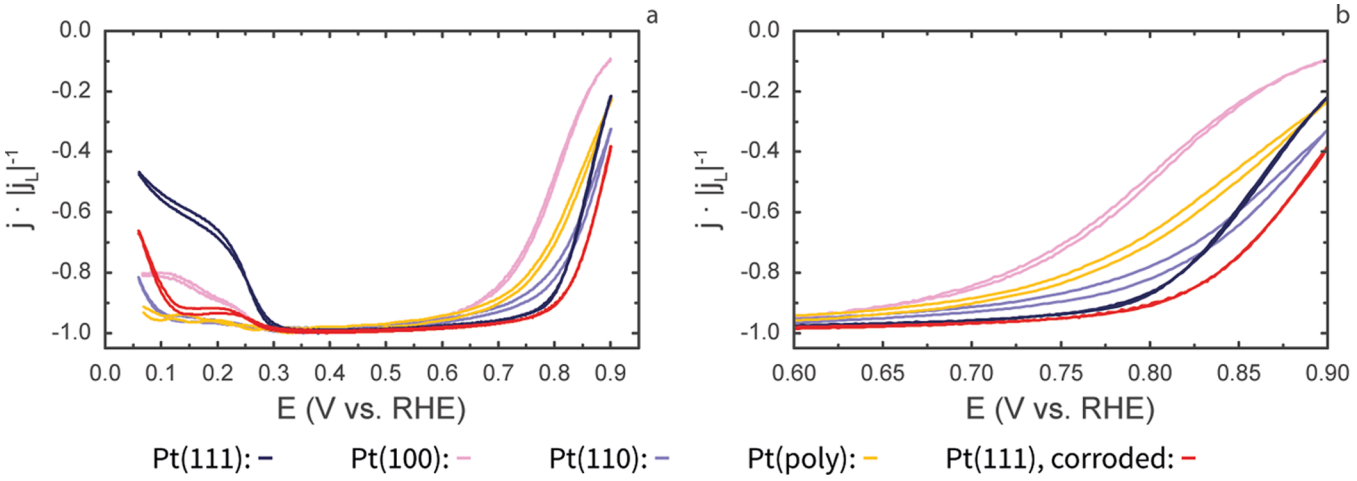

Figure 2. Cyclic voltammograms for oxygen reduction on Pt(111), Pt(100), Pt(110), Pt(poly), and Pt(111), which were corroded at -0.6 V vs RHE in 1 M NaOH. Both panels display the same data, in either the full scan range (a) or between 0.6 and 0.9 V vs RHE (b). The electrode rotation rate was 1600 rpm. Voltammograms were recorded in oxygen-saturated 0.1 M $HClO_4$ at a scan rate of 50 $mV \cdot s^{-1}$. Displayed voltammograms are the second voltammograms for each electrode at a 1600 rpm rotation rate, which overlaps well with the corresponding first voltammogram at 1600 rpm.

*OH bond weakening can be achieved by tuning the surface structure of platinum, for which the structure-sensitivity of ORR catalysis is well-documented: in $HClO_4$, the three Pt basal planes increase in activity in the order (100) < (111) < (110).[44] Even more active are stepped surfaces,[36,37,45] which contain concave sites at the bottom of each step which bind *OH weaker than Pt(111).[32] Notably though, most of these concave sites bind *OH slightly too weakly and thus overshoot the activity optimum for the ORR.[31] Instead, optimal activity can be achieved by removing atoms from flat platinum surfaces to create sites that bind *OH nearly optimally.[31,33]

Atom removal to optimize *OH binding may be achieved by cathodic corrosion because previous work identified the creation of etch pits during cathodic corrosion.[28,30] Although these roughly 30-nm-wide pits are larger than the optimal 1-nm-wide pits,[31] our previous work also indicates the presence of smaller etching features that are undetectable in scanning electron microscopy.[28,30,46] In fact, concave defects were recently incorporated during cathodic corrosion-based nanoparticle synthesis.[47] In an effort to generate these optimized concave sites on existing electrocatalysts, this section focuses on modifying Pt(111) through mild cathodic corrosion in 1 M NaOH.

First, as in previous work,[28,30] blank cyclic voltammograms of corroded and uncorroded Pt(111) were recorded. These CV curves are presented first. Then, the activity of the Pt(111) electrode was studied in the HMRD configuration.[24] Activity measurements will be presented after discussing cyclic voltammograms of corroded and uncorroded Pt(111).

Blank CV curves of Pt(111), before and after cathodic polarization in 1 M NaOH, are presented in Figure 1. As can be seen, the uncorroded Pt(111) electrode (in blue) contains the characteristic hydrogen adsorption and desorption features between 0.06 and 0.4 V versus RHE, followed by the double layer region and subsequent adsorption and desorption of OH between 0.5 and 0.9 V versus RHE.[48] Importantly, no peaks are visible at 0.13 and 0.29 V versus RHE. This indicates that no electrochemically observable step sites are present on the electrode before cathodic polarization.[49]

No additional peaks are present after polarizing Pt(111) at −0.5 V versus RHE in 1 M NaOH (Figure 1a). This indicates no change in the electrode structure when polarizing the electrode before the cathodic corrosion onset potential. In contrast, pronounced changes are visible after polarizing the electrode at the onset potential found in previous work: −0.6 V versus RHE (Figure 1b).[30] This treatment causes the formation of both (110) steps (0.13 V versus RHE) and (100) steps (0.29 V versus RHE). These changes indicate modest electrode roughening, as is indicated in Figure 1b by a 12% increase in the hydrogen desorption charge and minor etching features in previous SEM characterization.[30] These changes appear to be largely independent of the corrosion potential, as is illustrated in Figure S3. Additionally, the onset of *OH adsorption has shifted positively by about 0.02 V, which indicates a slightly weakened *OH adsorption strength on the (111) terrace of the corroded surface.[31] Such a weakened binding should promote the ORR activity for the corroded electrode.

The ORR activity is assessed in the HMRD configuration.[40] This configuration differs from the conventional rotating disk electrode (RDE) configuration because the working electrode is not encased in a shaft and submerged into the working solution. Instead, the bead- or cylinder-type crystal is mounted in a modified RDE rotator, and contact with the side of the electrode is prevented by elevating the electrode into a hanging meniscus configuration. Although this configuration allows for the convenient use of standard single crystal electrodes, care has to be taken to make sure that the HMRD behaves like a classical RDE electrode. This is indeed the case for most electrodes in the present study, as is discussed in the Supporting Information. The exception to this statement is Pt(110), which exhibited an apparent decrease in active surface area. This decrease is compensated for when presenting activity data in the main text. The HMRD setup can therefore be used to quantify the effect of cathodic corrosion on the ORR activity of Pt(111).

The ORR activity for a corroded Pt(111) electrode, a polycrystalline electrode, and the three basal planes of platinum is displayed in Figure 2. In this plot, all currents

https://dx.doi.org/10.1021/acscatal.0c04016
ACS Catal. 2020, 10, 15104−15113

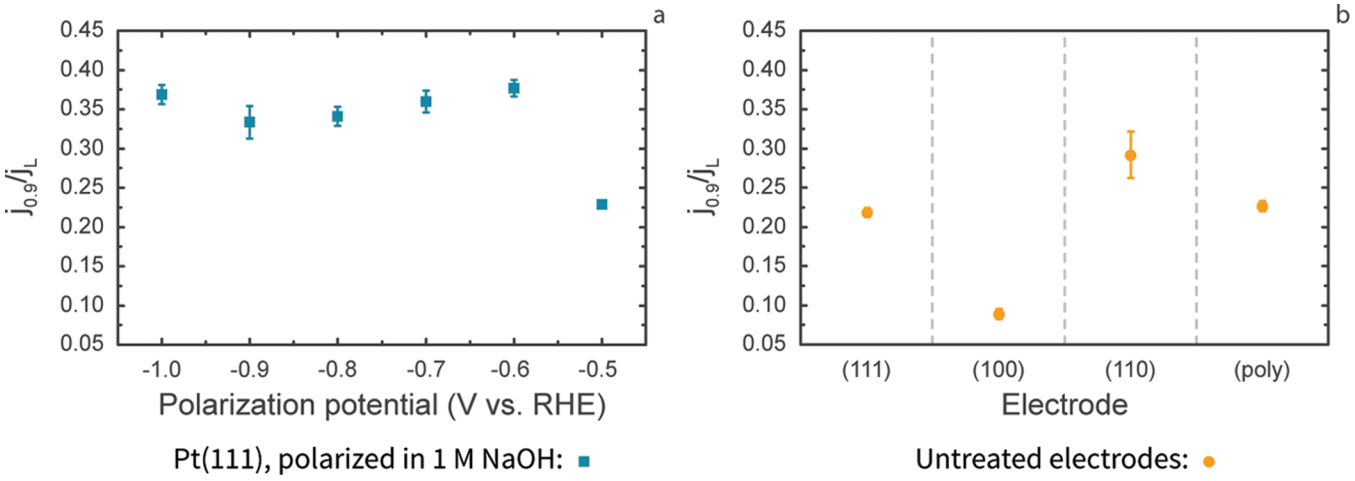

Figure 3. Normalized ORR activity of corroded Pt(111) as a function of the polarization potential (a) (blue squares) and of uncorroded electrodes (yellow circles) (b). Rotation rate: 1600 rpm. Each data point is the average of 3 or more experiments. Error bars represent one standard deviation.

are normalized by dividing by the absolute limiting current density for each electrode. This normalization accounts for minor variations in the limiting current due to small variations in the meniscus height[45] and small deviations in the alignment of the electrode.[17] The normalization therefore allows for objective comparison of the ORR activity in the HMRD configuration.[45]

As can be seen in Figure 2, the ORR activity at 0.9 V versus RHE follows the order Pt(100) < Pt(111) < Pt(110). This activity trend is in good agreement with both experimental results and recent density functional theory calculations.[31,32,44,50] A similar activity is achieved for Pt(poly), which has comparable activity to Pt(111). However, the corroded Pt(111) electrode is more active than all of the other studied crystals. This indicates that cathodic corrosion is indeed able to enhance the ORR activity of a Pt(111) electrode.

This enhancement is not only visible in the ORR voltammograms at 0.9 V versus RHE but also below 0.3 V versus RHE. At these potentials, Pt(111) suffers from ORR inhibition due to adsorbed hydrogen. This adsorbed hydrogen prevents most oxygen from being reduced to water, thus producing hydrogen peroxide instead.[37] Because hydrogen peroxide production requires two less electrons than water production from oxygen, the reduction current drops at potentials below 0.3 V versus RHE. This catalytic inhibition is generally alleviated by the introduction of step sites on the working electrode,[37] which matches the present observation for corroded Pt(111).

The activity enhancement through cathodic corrosion is more readily apparent from the quantitative activity assessment in Figure 3. In Figure 3, the absolute normalized current at 0.9 V is plotted for each electrode. In Panel b of this Figure, the activity of both Pt(111) and (100) shows excellent quantitative agreement with well-prepared electrodes from the work from Feliu et al., for which normalized activities of ∼0.21 (Pt(111)) and ∼0.09 (Pt(100)) were reported.[50] A more qualitative agreement is obtained for Pt(poly) and Pt(110), which are respectively more and less active than similar previously studied electrodes.[50,51] The increased Pt(poly) activity (with respect to an literature-extracted normalized activity of ∼0.19)[51] can be ascribed to a slightly different state of the surface, which can be expected for different polycrystalline electrodes. Similarly, the reduced activity of Pt(110) (with respect to a reported value of ∼0.32)[50] is caused by the crystal's high sensitivity to reconstructed 1 × 2 domains on the surface: if fewer reconstructed domains are formed during the cooling of the crystal, the ORR activity is reduced as well.[52] This remarkable sensitivity of Pt(110) to variations in the crystal cooling conditions is also responsible for the slightly larger error bar for Pt(110) in Figure 3b. From Panel b, it therefore appears that all electrodes are as active as expected from the literature.

With all uncorroded single crystals behaving in accordance with previous literature, the activity of cathodically treated Pt(111) can be assessed quantitatively (Figure 3a). In Figure 3a, it can be seen that the activity of Pt(111) is not enhanced if the polarization potential is less negative than the onset potential that was established in previous work.[30] However, the Pt(111) ORR activity increases sharply after cathodic treatment at or below the onset potential of −0.6 V versus RHE: the normalized activity improves from 0.22 to 0.38. This improvement corresponds to an increase in the kinetic current density (j_k) from 2.8 to 6.6 mA·cm^{-2}, as can be seen in Figure S6. This enhancement of both j_k and the normalized activity decreases slightly at more negative corrosion potentials but increases again to 0.37 (6.4 mA·cm^{-2}) at −1.0 V versus RHE. The oxygen reduction activity of Pt(111) can therefore be enhanced markedly through cathodic corrosion in 1 M NaOH.

Glycerol Oxidation. The second reaction of interest in this study is glycerol oxidation. Glycerol is an important byproduct of biodiesel production. As such, the affordability of glycerol as a feedstock has increased in tandem with biodiesel production.[53] The electrochemical valorization of glycerol to a variety of useful molecules is therefore a relevant field of research.[54] Unfortunately, glycerol oxidation typically results in a variety of reaction products.[55] For this reason, steering the selectivity of glycerol oxidation is of prime importance.

Enhanced selectivity can be achieved through surface tuning of Pt electrocatalysts because the electrocatalytic behavior of Pt varies for each type of surface site.[34,54,56] Introducing sites such as small defects on well-defined Pt(111) and Pt(100) electrodes has been linked to altered activity and selectivity in H_2SO_4 electrolytes.[57,58] Additionally, the selectivity for glycerol oxidation was recently shown to be different for Pt(111) and Pt(100): Pt(111) oxidizes the primary and

https://dx.doi.org/10.1021/acscatal.0c04016
ACS Catal. 2020, 10, 15104−15113

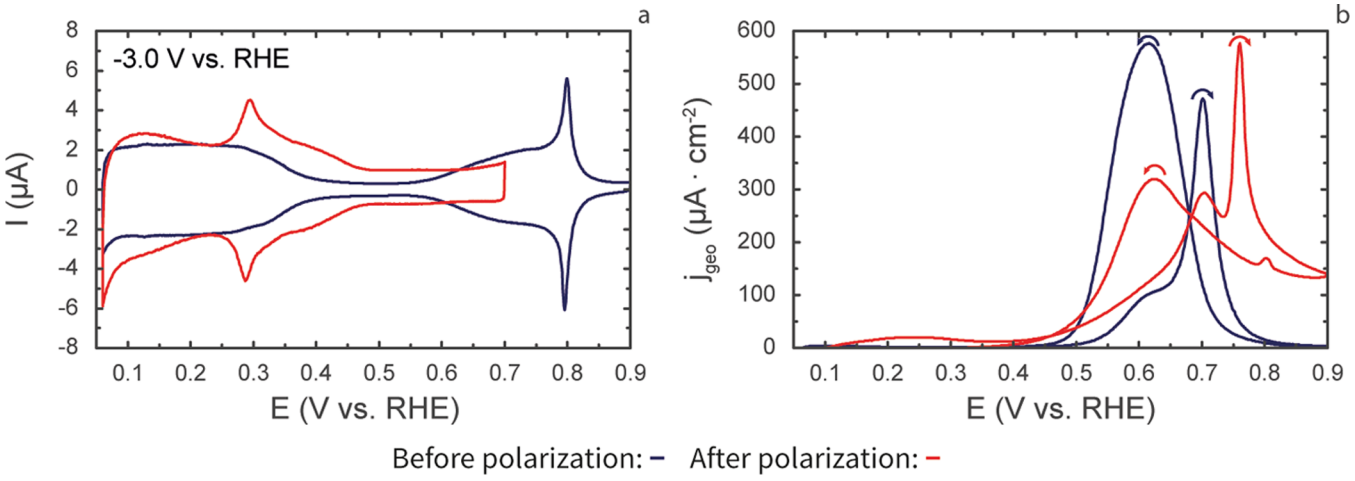

Figure 4. Blank cyclic voltammograms of Pt(111) before (blue trace) and after (red trace) cathodic polarization in 10 M NaOH at −3.0 V vs RHE (a) and glycerol oxidation voltammograms of the same electrodes (b). Blank voltammograms were recorded in 0.1 M $HClO_4$, at a scan rate of 50 mV·s^{-1}. Glycerol oxidation voltammograms were recorded in 0.5 M $HClO_4$ with 0.1 M glycerol at 10 mV·s^{-1}. For glycerol oxidation, the second voltammogram is displayed for each sample.

secondary hydroxyl groups of glycerol to form glyceraldehyde and dihydroxyacetone, respectively, while Pt(100) exclusively produces glyceraldehyde.[34] Based on these morphology-dependent selectivity differences, we will demonstrate how to alter the selectivity of Pt(111) by creating extended (100) terraces through cathodic corrosion.

To this end, cathodic corrosion was performed in 10 M NaOH. This concentrated electrolyte was chosen because previous work demonstrated the creation of well-defined (100) terraces when corroding polycrystalline Pt electrodes in this electrolyte.[28,30,46] Such extended terraces were required for altering the glycerol oxidation selectivity in 0.5 M $HClO_4$; creating only step sites through mild corrosion in more dilute electrolytes produced little to no electrochemically detectable selectivity changes (Figure S7).

The effect of extensive corrosion in 10 M NaOH is illustrated by the cyclic voltammograms in Figure 4a. These voltammograms reveal the creation of more surface area, as is apparent from the roughly threefold increase in the "double layer" current at 0.5 V versus RHE. The morphology of this increased surface area has been mapped extensively through scanning electron microscopy and atomic force microscopy in previous work.[28,30,46] Although part of the created surface area corresponds to (110) steps (0.13 V vs RHE), the majority of the area increase corresponds to the creation of (100) steps and terraces: the sharp peak at 0.29 V versus RHE corresponds to step formation, whereas the broad feature at higher potentials matches the formation of extended (100) terraces.[49]

Such terraces cause a marked change in the glycerol oxidation voltammograms, as displayed in Figure 4b. In this Figure, the second consecutive glycerol oxidation CV is displayed for each sample. These second cycles matched their corresponding first cycles, but exhibit clearer features because of the absence of additional oxidation features that are commonly seen during the first cycle.[56] In the glycerol oxidation voltammograms, untreated Pt(111) exhibits a sharp peak at 0.70 V versus RHE in the positive-going scan and a broader peak at 0.62 V versus RHE in the negative-going scan. Although these peaks are also present for the cathodically treated Pt(111), they have diminished in intensity and are now accompanied by a peak at 0.76 V versus RHE in the positive-going scan and a shoulder around 0.69 V versus RHE in the negative-going scan. These additional peaks and shoulders are likely caused by the newly formed (100) terraces, as Pt(100) catalyzes glycerol oxidation at higher potentials than Pt(111).[34,54,56]

This hypothesis is explored further through online HPLC of corroded and uncorroded Pt(111). Online HPLC is able to detect the products formed during glycerol oxidation and can therefore identify whether cathodically corroded Pt(111) contains catalytically active (100) terraces: Pt(100) produces only glyceraldehyde during the first step of glycerol oxidation in 0.5 M $HClO_4$, whereas Pt(111) also produces dihydroxyacetone.[34] An increase in Pt(100) sites should therefore lead to increased glyceraldehyde detection and less dihydroxyacetone detection through online HPLC.

HPLC results for corroded and uncorroded Pt(111) are presented in Figure 5, alongside glycerol oxidation linear sweep voltammograms. Both the HPLC and voltammetry results were recorded at a scan rate of 1 mV·s^{-1}, 10-fold slower than in Figure 4. At these scan rates, the glycerol oxidation voltammograms in Figure 5 for uncorroded Pt(111) exhibit a peak between 0.60 and 0.65 V versus RHE. The positive-going peak correlates with the detection of both dihydroxyacetone and glyceraldehyde in HPLC (Figure 5, Panel B and C). The HPLC-determined product concentrations are slightly delayed with regard to the electrochemical current. We attribute this delay to electrochemistry detecting product formation *rates*, whereas HPLC detects product *concentrations*. Because it takes a small amount of time to produce a given product concentration, a brief time delay is expected. The magnitude of this time delay depends on the distance of the HPLC sample collection tip to the electrode surface and the rate of product collection. Both this brief delay and the product concentration profiles for uncorroded Pt(111) agree well with previously published data.[34]

Voltammetry and HPLC data are markedly different for cathodically corroded Pt(111). This electrode exhibits a peak at more positive potentials in Figure 5a, matching the data presented for higher scan rates in Figure 4. This peak is located between 0.70 and 0.75 V versus RHE at a scan rate of 1 mV s^{-1}, where previous work detected activity for Pt(100)

https://dx.doi.org/10.1021/acscatal.0c04016
ACS Catal. 2020, 10, 15104−15113

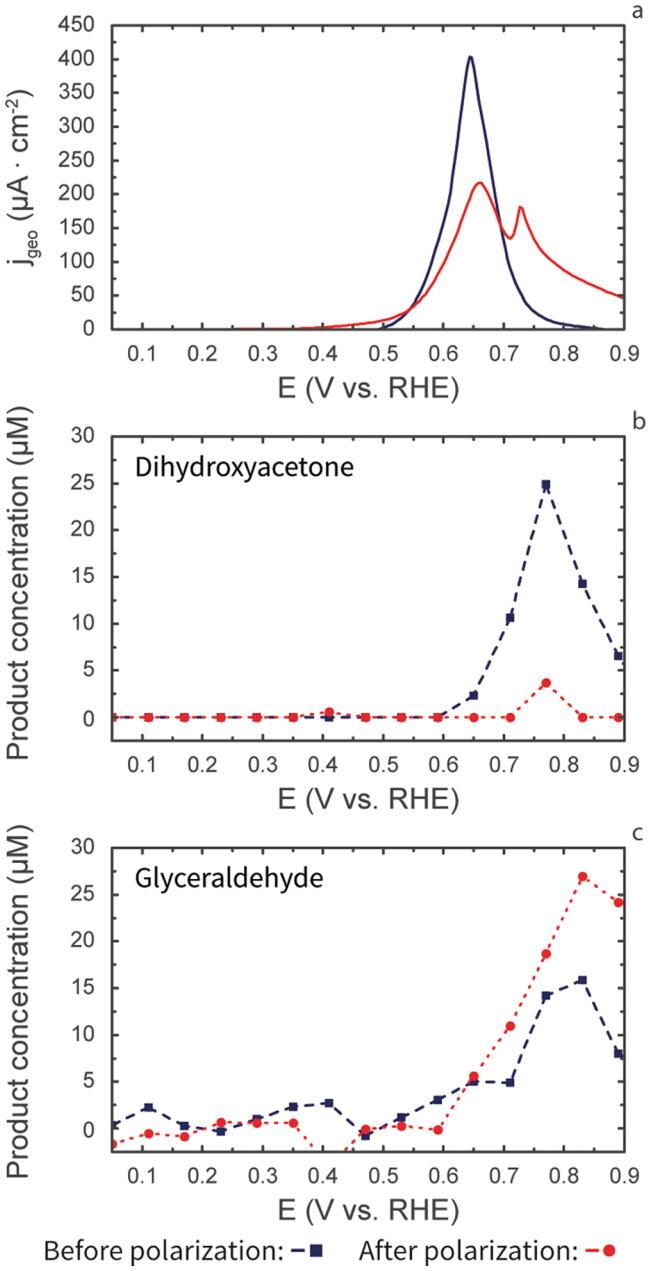

Figure 5. Glycerol oxidation voltammograms of Pt(111) before (blue trace) and after (red trace) cathodic polarization in 10 M NaOH at −3 V vs RHE (a) and concentration of dihydroxyacetone (b) and glyceraldehyde (c), as determined through online HPLC. Data were recorded in 0.5 M $HClO_4$ with 0.1 M glycerol at 1 mV·s^{-1}. Glyceraldehyde concentrations are baseline-corrected to account for ∼10 μM background signal. Because the cathodic corrosion voltage was not IR-corrected, a "real" corrosion potential of −2 V vs RHE was determined after cathodic corrosion.

electrodes.[34] Also matching the behavior of Pt(100) is the suppressed production of dihydroxyacetone during glycerol oxidation. Additionally, the selectivity towards glyceraldehyde production is higher for corroded Pt(111) than for uncorroded Pt(111). The increased glyceraldehyde formation and reduced in dihydroxyacetone formation both indicate that cathodic corrosion shifts the glycerol oxidation behavior of Pt(111) to resemble the behavior of Pt(100).

DISCUSSION

The previous sections have demonstrated that both the glycerol oxidation selectivity and the oxygen reduction activity of Pt(111) can be tailored through cathodic corrosion. We shall now briefly discuss the underlying cause of these catalytic changes. This discussion will follow our Results section in first addressing the ORR, followed by the glycerol oxidation reaction.

Oxygen Reduction. The ORR activity of Pt(111) can be more than doubled through cathodic electrode pretreatment, as is indicated by Figures 3 and S6. One might wonder whether the improvement is simply caused by the creation of step sites or by the formation of sites with optimal generalized coordination numbers.

The presence of step sites on Pt(111) is known to enhance the ORR activity.[36,37,45] If the presence of "normal" (110) and (100) step sites were the cause of the presently reported activity enhancement, the enhancement should therefore correlate roughly to the density of steps.[45] However, the step sites created by our method appear to have a much higher activity than most stepped single crystals:[50] only crystals with very high step densities surpass the normalized activity of the corroded electrodes. For example, our most active electrodes are as active as Pt(332), which has one (110) step for every five (111) terrace atoms[59] and a normalized activity of 0.38.[50] By qualitatively comparing the CV curves of Pt(332) and other stepped single crystals with those in Figure 1, one can conclude that the stepped crystals possess a much higher step density than the amount of defects on our corroded (111) electrodes.[59,60] Because our corroded Pt(111) matches the activity of Pt(332) while possessing a markedly lower step/defect density, it can be concluded that the corroded Pt(111) possesses a higher step-based ORR turnover frequency.

The lower ORR turnover frequency on stepped single crystals is likely due to those steps binding *OH too weakly and thus overshooting the per-step ORR activity optimum.[31] Because these steps are less active than the sites created in the current work, it appears that the presently created sites possess a more optimized *OH binding strength. Indeed, the cathodically created sites are approximately as active as "optimized" binding sites that can be created through anodic cycling.[31] Through such cycling, a 15% surface area increase through active site formation led to a current densities of approximately 7.4 mA·cm^{-2}. Such area increases and current densities are comparable to those presented here. It is therefore likely that both the previously reported anodically created sites[31] and the currently presented cathodically created sites have similar concave geometries with optimized *OH binding.[31−33]

A final argument for this conclusion is that optimized concave sites on single crystals are rather small,[31,33] being approximately 3 atoms (∼0.9 nm)[61] wide and having the optimally coordinated atom at the bottom of the pit. A high density of such sites should only be present after mild cathodic corrosion, for which no large features were detectable in SEM in previous work and the corresponding Supporting Information.[30] Accordingly, more pronounced corrosion will create overlapping etch pits that are readily visible in SEM and atomic force microscopy (AFM).[46] These pits contain fewer optimally coordinated Pt atoms per square nanometer and therefore *decrease* the ORR activity when adding step sites. This is indeed the case, as is demonstrated in the final section

https://dx.doi.org/10.1021/acscatal.0c04016
ACS Catal. 2020, 10, 15104−15113

of the Supporting Information. It is therefore likely that the presented ORR enhancements are caused by forming optimally sized catalytic sites.

Glycerol Oxidation. In contrast with the ORR, it is not the catalytic activity but the selectivity that is altered for glycerol oxidation: cathodic pretreatment in 10 M NaOH alters the product distribution of a Pt(111) catalyst.

Importantly, these changes are not caused by the formation of step sites, which have been shown to suppress the production of dihydroxyacetone during glycerol oxidation in 0.5 M H_2SO_4.[58] Such step sites play a negligible role in the current study, as is demonstrated in Figure S7. This apparent discrepancy between the current work in 0.5 M $HClO_4$ and previous work in 0.5 M H_2SO_4 can tentatively be explained by the difference in anion adsorption strength between both electrolytes: (bi)sulfate adsorbs more strongly than perchlorate.[38] As such, disruption of anion adsorption by step site introduction will likely affect catalysis more strongly for sulfate-based electrolytes than for perchlorate-based electrolytes. A similar mechanism is thought to underlie ORR activity differences between sulfuric acid and perchloric acid electrolytes.[36−38,62,63]

Having addressed the apparent discrepancy between the role of defects in 0.5 M H_2SO_4 and 0.5 M $HClO_4$, we can now discuss the role of extended Pt(100) terraces in enhancing selectivity towards glyceraldehyde. (100) sites cover a large part of the corroded electrode in Figure 4, as is indicated by an absolute charge increase of 89 $\mu C \cdot cm_{geo}^{-1}$ (2.2 times relative increase) between 0.25 and 0.50 V versus RHE in the blank voltammogram. Such (100) sites are prominent enough to be visible in SEM and AFM.[46] Though some additional (110) sites are also visible below 0.25 V versus RHE in Figure 4a (12 $\mu C \cdot cm_{geo}^{-1}$ increase), the newly formed (100) domains appear to dominate the glycerol oxidation behavior.

In fact, the corroded electrode behaves similarly to Pt(100) single crystals,[34] as is suggested by the CV and HPLC results in Figure 5. Like Pt(100) crystals, our corroded electrodes exhibit a current maximum at higher potentials than pristine Pt(111). Additionally, Pt(100) single crystals produce no dihydroxyacetone and instead solely generate glyceraldehyde.[34] This behavior parallels the increased glyceraldehyde production and diminished overall dihydroxyacetone production after cathodically introducing Pt(100) sites. In other words, cathodically created (100) terraces shift the catalytic behavior of a Pt(111) electrode towards that of a Pt(100) electrode. This observation aligns with previous suggestions that the various crystal facets of platinum oxidize glycerol independently.[56] We therefore conclude that the improved selectivity towards glyceraldehyde after cathodic corrosion is caused by the replacement of the (111) terraces by extended the (100) terraces.

Outlook. Based on the aforementioned considerations, it appears that cathodic corrosion is suitable for creating more active ORR sites and more selective glycerol oxidation sites on a Pt(111) electrode. One should note that these results are a proof of concept, demonstrated by applying cathodic corrosion in a clean system and on a well-defined electrode; better results might be obtained when optimizing different catalysts and employing different conditions for cathodic corrosion, ideally directed by previously outlined recommendations for applying cathodic corrosion.[30] In optimizing corrosion, one should note that varying the corrosion electrolyte appears more effective in modifying Pt electrodes than varying the corrosion time length: below 15 min, the cathodically created surface distribution does not vary strongly for a given corrosion electrolyte.[30,46]

Because our approach can be optimized in various manners, our results open possibilities for optimizing both randomly and preferentially oriented nanocatalysts for a variety of structure-sensitive reactions.[21,23,24] Although modifying nanocatalysts will require overcoming challenges such as nanoparticle detachment from the support during cathodic corrosion, such a modification might be a viable strategy for producing industrially relevant electrocatalysts. Importantly, hydrogen-induced nanoparticle detachment or etching-induced material dissolution can be quantified using presently available techniques.[64] Such quantification should prove useful in optimizing cathodic corrosion for nanocatalyst tailoring.

Additionally, electrocatalysts can be "regenerated" through cathodic corrosion because a brief period of cathodic corrosion and the accompanying hydrogen evolution might remove catalyst contaminants and counteract detrimental catalyst shape changes that can be caused by standard catalyst operation and storage.[65] The role of cathodic corrosion in catalyst regeneration and synthesis is further encouraged by recent results, where cathodic corrosion in methanol was shown to improve the distribution of various types of metallic nanoparticles.[66]

CONCLUSIONS

Summarizing, this article has demonstrated that the oxygen reduction activity and glycerol oxidation selectivity of Pt(111) can be significantly altered by cathodic corrosion. These modifications are respectively caused by the formation of optimally sized ORR sites and extended (100) terraces. Each of these morphologies can be created by selecting the appropriate cathodic corrosion conditions, thus leveraging previously established electrolyte effects. These results strongly support the possible use of cathodic corrosion to both pretreat and regenerate metallic nanoparticles for optimized catalytic activity and selectivity. As such, cathodic corrosion could be a powerful tool in future electrocatalyst improvement.

ASSOCIATED CONTENT

Supporting Information

The Supporting Information is available free of charge at https://pubs.acs.org/doi/10.1021/acscatal.0c04016.

Blank electrode voltammograms before and after corrosion; HMRD setup validation; kinetic ORR current densities; glycerol oxidation after mild corrosion; and ORR after more severe corrosion (PDF)

AUTHOR INFORMATION

Corresponding Authors

Thomas J. P. Hersbach − *Leiden Institute of Chemistry, Leiden University, 2300 RA Leiden, The Netherlands;* orcid.org/0000-0001-5467-6151; Email: hersbach@slac.stanford.edu

Marc T. M. Koper − *Leiden Institute of Chemistry, Leiden University, 2300 RA Leiden, The Netherlands;* orcid.org/0000-0001-6777-4594; Email: m.koper@lic.leidenuniv.nl

Authors

Chunmiao Ye − *Leiden Institute of Chemistry, Leiden University, 2300 RA Leiden, The Netherlands*

Amanda C. Garcia − *Leiden Institute of Chemistry, Leiden University, 2300 RA Leiden, The Netherlands;* orcid.org/0000-0002-0242-9244

Complete contact information is available at: https://pubs.acs.org/10.1021/acscatal.0c04016

Notes

The authors declare no competing financial interest.

■ ACKNOWLEDGMENTS

The authors thank Magneto Special Anodes for providing dimensionally stable anode counter electrodes. They additionally gratefully acknowledge prof. Juan M. Feliu for useful discussions on the oxygen reduction activity of Pt(110) electrodes.

■ REFERENCES

(1) Anderson, K.; Peters, G. The Trouble with Negative Emissions. *Science* **2016**, *354*, 182−183.
(2) Oreskes, N. The Scientific Consensus on Climate Change: How Do We Know We're Not Wrong? In *Climate Modelling*; Lloyd, E. A., Winsberg, E., Eds.; Palgrave Macmillan: Cham, 2018; pp 31−64.
(3) Grey, C. P.; Tarascon, J. M. Sustainability and in Situ Monitoring in Battery Development. *Nat. Mater.* **2017**, *16*, 45−56.
(4) Bockris, J. O. Hydrogen Economy. *Science* **1972**, *176*, 1323.
(5) Katsounaros, I.; Koper, M. T. M. Electrocatalysis for the Hydrogen Economy. *Electrochemical Science for a Sustainable Society*; Springer International Publishing: Cham, 2017; pp 23−50.
(6) Glenk, G.; Reichelstein, S. Economics of Converting Renewable Power to Hydrogen. *Nat. Energy* **2019**, *4*, 216−222.
(7) De Luna, P.; Hahn, C.; Higgins, D.; Jaffer, S. A.; Jaramillo, T. F.; Sargent, E. H. What Would It Take for Renewably Powered Electrosynthesis to Displace Petrochemical Processes? *Science* **2019**, *364*, No. eaav3506.
(8) Perathoner, S.; Centi, G. Catalysis for Solar-Driven Chemistry: The Role of Electrocatalysis. *Catal. Today* **2019**, *330*, 157−170.
(9) Kyriakou, V.; Garagounis, I.; Vourros, A.; Vasileiou, E.; Stoukides, M. An Electrochemical Haber-Bosch Process. *Joule* **2020**, *4*, 142−158.
(10) Seh, Z. W.; Kibsgaard, J.; Dickens, C. F.; Chorkendorff, I.; Nørskov, J. K.; Jaramillo, T. F. Combining Theory and Experiment in Electrocatalysis: Insights into Materials Design. *Science* **2017**, *355*, No. eaad4998.
(11) Gilroy, K. D.; Ruditskiy, A.; Peng, H.-C.; Qin, D.; Xia, Y. Bimetallic Nanocrystals: Syntheses, Properties, and Applications. *Chem. Rev.* **2016**, *116*, 10414−10472.
(12) He, J.; Johnson, N. J. J.; Huang, A.; Berlinguette, C. P. Electrocatalytic Alloys for CO2 Reduction. *ChemSusChem* **2018**, *11*, 48−57.
(13) Kulkarni, A.; Siahrostami, S.; Patel, A.; Nørskov, J. K. Understanding Catalytic Activity Trends in the Oxygen Reduction Reaction. *Chem. Rev.* **2018**, *118*, 2302−2312.
(14) Andersen, M.; Medford, A. J.; Nørskov, J. K.; Reuter, K. Scaling-Relation-Based Analysis of Bifunctional Catalysis: The Case for Homogeneous Bimetallic Alloys. *ACS Catal.* **2017**, *7*, 3960−3967.
(15) Stamenkovic, V. R.; Fowler, B.; Mun, B. S.; Wang, G.; Ross, P. N.; Lucas, C. A.; Markovic, N. M. Improved Oxygen Reduction Activity on Pt3Ni(111) via Increased Surface Site Availability. *Science* **2007**, *315*, 493−497.
(16) Stamenkovic, V. R.; Mun, B. S.; Arenz, M.; Mayrhofer, K. J. J.; Lucas, C. A.; Wang, G.; Ross, P. N.; Markovic, N. M. Trends in Electrocatalysis on Extended and Nanoscale Pt-Bimetallic Alloy Surfaces. *Nat. Mater.* **2007**, *6*, 241−247.
(17) Wakisaka, M.; Kobayashi, S.; Morishima, S.; Hyuga, Y.; Tryk, D. A.; Watanabe, M.; Iiyama, A.; Uchida, H. Unprecedented Dependence of the Oxygen Reduction Activity on Co Content at Pt Skin/Pt-Co(111) Single Crystal Electrodes. *Electrochem. Commun.* **2016**, *67*, 47−50.
(18) Hahn, C.; Abram, D. N.; Hansen, H. A.; Hatsukade, T.; Jackson, A.; Johnson, N. C.; Hellstern, T. R.; Kuhl, K. P.; Cave, E. R.; Feaster, J. T.; Jaramillo, T. F. Synthesis of Thin Film AuPd Alloys and Their Investigation for Electrocatalytic CO 2 Reduction. *J. Mater. Chem. A* **2015**, *3*, 20185−20194.
(19) Stephens, I. E. L.; Bondarenko, A. S.; Grønbjerg, U.; Rossmeisl, J.; Chorkendorff, I. Understanding the Electrocatalysis of Oxygen Reduction on Platinum and Its Alloys. *Energy Environ. Sci.* **2012**, *5*, 6744.
(20) Greeley, J.; Nørskov, J. K. Combinatorial Density Functional Theory-Based Screening of Surface Alloys for the Oxygen Reduction Reaction. *J. Phys. Chem. C* **2009**, *113*, 4932−4939.
(21) Strasser, P.; Gliech, M.; Kuehl, S.; Moeller, T. Electrochemical Processes on Solid Shaped Nanoparticles with Defined Facets. *Chem. Soc. Rev.* **2018**, *47*, 715−735.
(22) Liao, H.; Fisher, A.; Xu, Z. J. Surface Segregation in Bimetallic Nanoparticles: A Critical Issue in Electrocatalyst Engineering. *Small* **2015**, *11*, 3221−3246.
(23) Koper, M. T. M. Structure Sensitivity and Nanoscale Effects in Electrocatalysis. *Nanoscale* **2011**, *3*, 2054−2073.
(24) Zaera, F. Shape-Controlled Nanostructures in Heterogeneous Catalysis. *ChemSusChem* **2013**, *6*, 1797−1820.
(25) Niu, Z.; Li, Y. Removal and Utilization of Capping Agents in Nanocatalysis. *Chem. Mater.* **2014**, *26*, 72−83.
(26) Tian, N.; Zhou, Z.-Y.; Sun, S.-G.; Ding, Y.; Wang, Z. L. Synthesis of Tetrahexahedral Platinum Nanocrystals with High-Index Facets and High Electro-Oxidation Activity. *Science* **2007**, *316*, 732−735.
(27) Yanson, A. I.; Rodriguez, P.; Garcia-Araez, N.; Mom, R. V.; Tichelaar, F. D.; Koper, M. T. M. Cathodic Corrosion: A Quick, Clean, and Versatile Method for the Synthesis of Metallic Nanoparticles. *Angew. Chem. Int. Ed.* **2011**, *50*, 6346−6350.
(28) Hersbach, T. J. P.; Yanson, A. I.; Koper, M. T. M. Anisotropic Etching of Platinum Electrodes at the Onset of Cathodic Corrosion. *Nat. Commun.* **2016**, *7*, 12653.
(29) Hersbach, T. J. P.; Mints, V. A.; Calle-Vallejo, F.; Yanson, A. I.; Koper, M. T. M. Anisotropic Etching of Rhodium and Gold as the Onset of Nanoparticle Formation by Cathodic Corrosion. *Faraday Discuss.* **2016**, *193*, 207−222.
(30) Hersbach, T. J. P.; McCrum, I. T.; Anastasiadou, D.; Wever, R.; Calle-Vallejo, F.; Koper, M. T. M. Alkali Metal Cation Effects in Structuring Pt, Rh, and Au Surfaces through Cathodic Corrosion. *ACS Appl. Mater. Interfaces* **2018**, *10*, 39363−39379.
(31) Calle-Vallejo, F.; Tymoczko, J.; Colic, V.; Vu, Q. H.; Pohl, M. D.; Morgenstern, K.; Loffreda, D.; Sautet, P.; Schuhmann, W.; Bandarenka, A. S. Finding Optimal Surface Sites on Heterogeneous Catalysts by Counting Nearest Neighbors. *Science* **2015**, *350*, 185−189.
(32) Calle-Vallejo, F.; Pohl, M. D.; Reinisch, D.; Loffreda, D.; Sautet, P.; Bandarenka, A. S. Why Conclusions from Platinum Model Surfaces Do Not Necessarily Lead to Enhanced Nanoparticle Catalysts for the Oxygen Reduction Reaction. *Chem. Sci.* **2017**, *8*, 2283−2289.
(33) Núñez, M.; Lansford, J. L.; Vlachos, D. G. Optimization of the Facet Structure of Transition-Metal Catalysts Applied to the Oxygen Reduction Reaction. *Nat. Chem.* **2019**, *11*, 449−456.
(34) Garcia, A. C.; Kolb, M. J.; van Nierop y Sanchez, C.; Vos, J.; Birdja, Y. Y.; Kwon, Y.; Tremiliosi-Filho, G.; Koper, M. T. M. Strong Impact of Platinum Surface Structure on Primary and Secondary Alcohol Oxidation during Electro-Oxidation of Glycerol. *ACS Catal.* **2016**, *6*, 4491−4500.
(35) Van de Krol, R. The Reference and Quasi-Reference Electrodes. In *Photoelectrochemical Hydrogen Production*; Van de Krol, R., Grätzel, M., Eds.; Springer: Boston, MA, 2012; p 109.
(36) Maciá, M. D.; Campiña, J. M.; Herrero, E.; Feliu, J. M. On the Kinetics of Oxygen Reduction on Platinum Stepped Surfaces in Acidic Media. *J. Electroanal. Chem.* **2004**, *564*, 141−150.

(37) Kuzume, A.; Herrero, E.; Feliu, J. M. Oxygen Reduction on Stepped Platinum Surfaces in Acidic Media. *J. Electroanal. Chem.* **2007**, *599*, 333−343.
(38) Attard, G. A.; Brew, A.; Hunter, K.; Sharman, J.; Wright, E. Specific Adsorption of Perchlorate Anions on Pt{hkl} Single Crystal Electrodes. *Phys. Chem. Chem. Phys.* **2014**, *16*, 13689−13698.
(39) Jung, S.; McCrory, C. C. L.; Ferrer, I. M.; Peters, J. C.; Jaramillo, T. F. Benchmarking Nanoparticulate Metal Oxide Electrocatalysts for the Alkaline Water Oxidation Reaction. *J. Mater. Chem. A* **2016**, *4*, 3068−3076.
(40) Villullas, H. M.; Teijelo, M. L. The Hanging-Meniscus Rotating Disk (HMRD) Part 1. Dependence of Hydrodynamic Behavior on Experimental Variables. *J. Electroanal. Chem.* **1995**, *384*, 25−30.
(41) Jiao, L.; Liu, E.; Mukerjee, S.; Jia, Q. In Situ Identification of Non-Specific Adsorption of Alkali Metal Cations on Pt Surfaces and Their Catalytic Roles in Alkaline Solutions. *ACS Catal.* **2020**, *10*, 11099−11109.
(42) Nørskov, J. K.; Rossmeisl, J.; Logadottir, A.; Lindqvist, L.; Kitchin, J. R.; Bligaard, T.; Jónsson, H. Origin of the Overpotential for Oxygen Reduction at a Fuel-Cell Cathode. *J. Phys. Chem. B* **2004**, *108*, 17886−17892.
(43) Markovic, N. Surface Science Studies of Model Fuel Cell Electrocatalysts. *Surf. Sci. Rep.* **2002**, *45*, 117−229.
(44) Marković, N. M.; Adžić, R. R.; Cahan, B. D.; Yeager, E. B. Structural Effects in Electrocatalysis: Oxygen Reduction on Platinum Low Index Single-Crystal Surfaces in Perchloric Acid Solutions. *J. Electroanal. Chem.* **1994**, *377*, 249−259.
(45) Gómez-Marín, A. M.; Feliu, J. M. Oxygen Reduction on Nanostructured Platinum Surfaces in Acidic Media: Promoting Effect of Surface Steps and Ideal Response of Pt(111). *Catal. Today* **2015**, *244*, 172−176.
(46) Arulmozhi, N.; Hersbach, T. J. P.; Koper, M. T. M. Nanoscale Morphological Evolution of Monocrystalline Pt Surfaces during Cathodic Corrosion. *Proc. Natl. Acad. Sci.* **2020**, In Press.
(47) Fichtner, J.; Watzele, S.; Garlyyev, B.; Kluge, R. M.; Haimerl, F.; El-Sayed, H. A.; Li, W.-J.; Maillard, F. M.; Dubau, L.; Chattot, R.; Michalička, J.; Macak, J. M.; Wang, W.; Wang, D.; Gigl, T.; Hugenschmidt, C.; Bandarenka, A. S. Tailoring the Oxygen Reduction Activity of Pt Nanoparticles through Surface Defects: A Simple Top-Down Approach. *ACS Catal.* **2020**, *10*, 3131−3142.
(48) Gomez, R.; Orts, J. M.; Alvarez-Ruiz, B.; Feliu, J. M. Effect of Temperature on Hydrogen Adsorption on Pt(111), Pt(110), and Pt(100) Electrodes in 0.1 M HClO4. *J. Phys. Chem. B* **2004**, *108*, 228−238.
(49) Vidal-Iglesias, F. J.; Arán-Ais, R. M.; Solla-Gullón, J.; Herrero, E.; Feliu, J. M. Electrochemical Characterization of Shape-Controlled Pt Nanoparticles in Different Supporting Electrolytes. *ACS Catal.* **2012**, *2*, 901−910.
(50) Gómez-Marín, A. M.; Rizo, R.; Feliu, J. M. Oxygen Reduction Reaction at Pt Single Crystals: A Critical Overview. *Catal. Sci. Technol.* **2014**, *4*, 1685.
(51) Gómez-Marín, A.; Feliu, J.; Edson, T. Reaction Mechanism for Oxygen Reduction on Platinum: Existence of a Fast Initial Chemical Step and a Soluble Species Different from H2O2. *ACS Catal.* **2018**, *8*, 7931−7943.
(52) Attard, G. A.; Brew, A. Cyclic Voltammetry and Oxygen Reduction Activity of the Pt{110}-(1×1) Surface. *J. Electroanal. Chem.* **2015**, *747*, 123−129.
(53) Rahmat, N.; Abdullah, A. Z.; Mohamed, A. R. Recent Progress on Innovative and Potential Technologies for Glycerol Transformation into Fuel Additives: A Critical Review. *Renew. Sustain. Energy Rev.* **2010**, *14*, 987−1000.
(54) Gomes, J. F.; de Paula, F. B. C.; Gasparotto, L. H. S.; Tremiliosi-Filho, G. The Influence of the Pt Crystalline Surface Orientation on the Glycerol Electro-Oxidation in Acidic Media. *Electrochim. Acta* **2012**, *76*, 88−93.
(55) Kwon, Y.; Koper, M. T. M. Combining Voltammetry with HPLC: Application to Electro-Oxidation of Glycerol. *Anal. Chem.* **2010**, *82*, 5420−5424.
(56) Fernández, P. S.; Martins, C. A.; Angelucci, C. A.; Gomes, J. F.; Camara, G. A.; Martins, M. E.; Tremiliosi-Filho, G. Evidence for Independent Glycerol Electrooxidation Behavior on Different Ordered Domains of Polycrystalline Platinum. *ChemElectroChem* **2015**, *2*, 263−268.
(57) Fernández, P. S.; Fernandes Gomes, J.; Angelucci, C. A.; Tereshchuk, P.; Martins, C. A.; Camara, G. A.; Martins, M. E.; Da Silva, J. L. F.; Tremiliosi-Filho, G. Establishing a Link between Well-Ordered Pt(100) Surfaces and Real Systems: How Do Random Superficial Defects Influence the Electro-Oxidation of Glycerol? *ACS Catal.* **2015**, *5*, 4227−4236.
(58) Fernández, P. S.; Tereshchuk, P.; Angelucci, C. A.; Gomes, J. F.; Garcia, A. C.; Martins, C. A.; Camara, G. A.; Martins, M. E.; Da Silva, J. L. F.; Tremiliosi-Filho, G. How Do Random Superficial Defects Influence the Electro-Oxidation of Glycerol on Pt(111) Surfaces? *Phys. Chem. Chem. Phys.* **2016**, *18*, 25582−25591.
(59) Armand, D.; Clavilier, J. Electrochemical Behaviour of the (110) Orientation of a Platinum Surface in Acid Medium: The Role of Anions. *J. Electroanal. Chem. Interfacial Electrochem.* **1989**, *263*, 109−126.
(60) Clavilier, J.; El Achi, K.; Rodes, A. In Situ Probing of Step and Terrace Sites on Pt(S)-[n(111) × (111)] Electrodes. *Chem. Phys.* **1990**, *141*, 1−14.
(61) Arblaster, J. W. Crystallographic Properties of Platinum. *Platin. Met. Rev.* **1997**, *41*, 12−21.
(62) Markovic, N. M.; Gasteiger, H. a.; Ross, P. N. Oxygen Reduction on Platinum Low-Index Single-Crystal Surfaces in Sulfuric Acid Solution: Rotating Ring-Pt(Hkl) Disk Studies. *J. Phys. Chem.* **1995**, *99*, 3411−3415.
(63) Xie, C.; Niu, Z.; Kim, D.; Li, M.; Yang, P. Surface and Interface Control in Nanoparticle Catalysis. *Chem. Rev.* **2020**, *120*, 1184−1249.
(64) Cherevko, S.; Zeradjanin, A. R.; Topalov, A. A.; Kulyk, N.; Katsounaros, I.; Mayrhofer, K. J. J. Dissolution of Noble Metals during Oxygen Evolution in Acidic Media. *ChemCatChem* **2014**, *6*, 2219−2223.
(65) Öhl, D.; Franzen, D.; Paulisch, M.; Dieckhöfer, S.; Barwe, S.; Andronescu, C.; Manke, I.; Turek, T.; Schuhmann, W. Catalytic Reactivation of Industrial Oxygen Depolarized Cathodes by in Situ Generation of Atomic Hydrogen. *ChemSusChem* **2019**, *12*, 2732−2739.
(66) Vanrenterghem, B.; Bele, M.; Zepeda, F. R.; Šala, M.; Hodnik, N.; Breugelmans, T. Cutting the Gordian Knot of Electrodeposition via Controlled Cathodic Corrosion Enabling the Production of Supported Metal Nanoparticles below 5 Nm. *Appl. Catal. B Environ.* **2018**, *226*, 396−402.

https://dx.doi.org/10.1021/acscatal.0c04016
ACS Catal. 2020, 10, 15104−15113